

Converging PMF Calculations of Antibiotic Permeation across an Outer Membrane Porin with Subkilocalorie per Mole Accuracy

Jeremy Lapierre and Jochen S. Hub*



Cite This: *J. Chem. Inf. Model.* 2023, 63, 5319–5330



Read Online

ACCESS |



Metrics & More

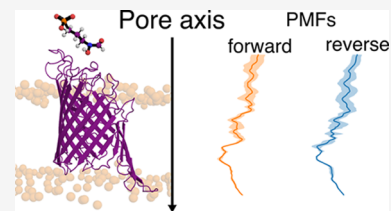


Article Recommendations



Supporting Information

ABSTRACT: The emergence of multidrug-resistant pathogens led to a critical need for new antibiotics. A key property of effective antibiotics against Gram-negative bacteria is their ability to permeate through the bacterial outer membrane via transmembrane porin proteins. Molecular dynamics (MD) simulations are, in principle, capable of modeling antibiotic permeation across outer membrane porins (OMPs). However, owing to sampling problems, it has remained challenging to obtain converged potentials of mean force (PMFs) for antibiotic permeation across OMPs. Here, we investigated the convergence of PMFs along a single collective variable aimed at quantifying the permeation of the antibiotic fosmidomycin across the OprO porin. We compared standard umbrella sampling (US) with three advanced flavors of the US technique: (i) Hamiltonian replica exchange with solute tempering in combination with US, (ii) simulated tempering-enhanced US, and (iii) replica-exchange US. To quantify the PMF convergence and to reveal hysteresis problems, we computed several independent sets of US simulations starting from pulling simulations in the outward and inward permeation directions. We find that replica-exchange US in combination with well-chosen restraints is highly successful for obtaining converged PMFs of fosmidomycin permeation through OprO, reaching PMFs converged to subkilocalorie per mole accuracy.



INTRODUCTION

Pseudomonas aeruginosa is a Gram-negative bacterium, which differs from Gram-positive bacteria in the presence of an outer membrane and of a thinner peptidoglycan layer (Figure 1). *P. aeruginosa* is an opportunistic pathogen, implying that it is usually not harmful to healthy individuals but may cause severe disease in hosts who suffer from a defective immune system or who are weakened by other diseases. For this reason, infections by *P. aeruginosa* are frequent in hospitals and, accordingly, classified as nosocomial infections.^{1–3} Pathogens causing nosocomial infections are often multidrug-resistant; this is specifically true for *P. aeruginosa*. The World Health Organization emphasized a critical need for new antibiotics against this group of pathogens to better protect hospitalized patients.⁴

Absorption of nutrients by *P. aeruginosa* from the extracellular medium is mediated by outer membrane porin proteins (Figure 1), which select the incoming molecules by their charge and size.^{5–7} To design new effective antibiotics, it is thus of paramount importance to take into account the permeability of porins for drug candidates. Notably, *P. aeruginosa* and *Acinetobacter baumannii* lack unspecific porins with larger pore diameters, thereby leading to lower outer membrane permeability for polar solutes as compared to Enterobacteriaceae.⁸ The lack of unspecific porins has been associated with particular drug resistance,^{7,9–11} although recent work emphasized the importance of direct permeation across the lipid membrane for drug uptake.¹² Detailed descriptions of bacterial outer membrane porins as well as permeation

mechanisms of small molecules through these molecular gateways have been reviewed in detail.^{13,14}

In this study, we focused on the permeation of fosmidomycin through OprO porin, a polyphosphate-specific homotrimeric transmembrane protein. Fosmidomycin is an inhibitor of the 1-deoxy-D-xylulose 5-phosphate reductoisomerase, an enzyme involved in a biosynthesis pathway for isoprenoids but specific to bacteria and protozoa. Isoprenoids play major roles in functions such as electron transport or cell signaling;¹⁵ therefore, blocking the bacterial specific pathway of isoprenoid biosynthesis is an effective strategy to impede the proliferation of the pathogen.

Atomistic molecular dynamics (MD) simulations have been used to estimate the permeability of bacterial porins for antibiotics by computing the free-energy landscape along the permeation pathway.^{16–23} However, such simulations are frequently subjected to considerable sampling challenges. The free-energy landscape, also referred to as the potential of mean force (PMF), has often been computed with methods such as umbrella sampling (US)²⁴ or metadynamics,²⁵ which require the definition of one or multiple collective variables (CVs). Golla et al. recently showed that PMF calculations

Received: June 11, 2023

Published: August 10, 2023



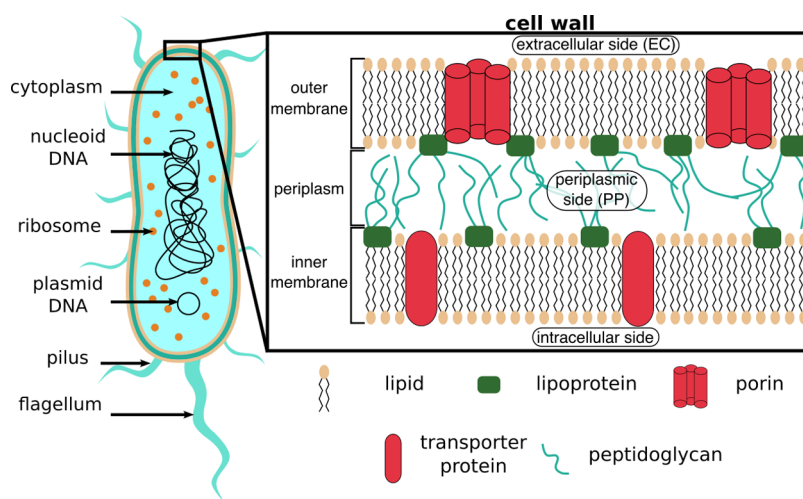


Figure 1. Overall structure and macromolecular components of *P. aeruginosa*, a Gram-negative bacterium. Outer membrane porins (red cylinders) constitute possible uptake pathways for antibiotics.

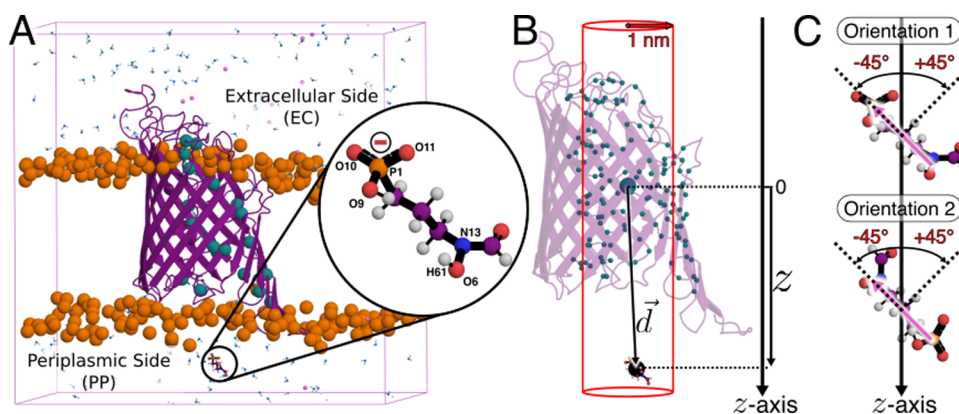


Figure 2. Setup for simulating fosmidomycin permeation through the OprO porin. (A) Simulation system. OprO is shown as a purple cartoon, POPE phosphate groups as orange spheres, key lysine and arginine residues along the porin contributing to its anionic selectivity are highlighted with cyan spheres, fosmidomycin and a few water molecules are represented as balls and sticks, and potassium cations are shown as small pink spheres. Most of the water molecules have been removed for clarity. The focus on fosmidomycin shows key atoms that have been used for defining the CV. (B) The large cyan bead depicts the center of mass of all C_{α} atoms close to the porin's lumen (pCOM) represented as small cyan beads. The large black sphere represents the center of mass of the following atoms in fosmidomycin: P1, O9–11, N13, H61, and O6 (fCOM). The z -component of the vector connecting the pCOM and the fCOM was used as the CV for driving the permeation process. The red cylinder illustrates the cylindrical flat-bottomed position restraint. (C) Two fosmidomycin's orientations studied in this work. The pink arrow represents the vector connecting COMs of the phosphoryl and amine groups; the angle between this vector and the z -axis has been restrained with a flat-bottom potential such that this angle is maintained within $[-45^{\circ}, +45^{\circ}]$.

based on standalone US using the drug position along the pore as the only CV suffer from major hysteresis effects,²⁶ whereas well-tempered metadynamics with multiple walkers along the same CV yielded more accurate PMFs.^{26,27} To improve the sampling of antibiotic orientation, metadynamics has furthermore been applied along two CVs, yielding the PMF as a function of solute position and solute orientation.^{27,28} Because standalone US frequently suffers from sampling and hysteresis problems, several improved flavors of US have been developed including Hamiltonian replica-exchange US,^{29–31} temperature-accelerated sliced sampling (TASS),³² and simulated tempering-enhanced umbrella sampling (STeUS).³³ In fact, replica-exchange US—a specific application of Hamiltonian replica-exchange simulations—has been successfully applied to obtain quantitative insight into antibiotic permeation through OprF.^{34,35} Acharya et al. applied TASS to rationalize the permeation of ciprofloxacin through OprF.³⁶ Furthermore, Vasan et al. analyzed the role of large-scale loop transitions in

OprF, which pose particular sampling challenges.³⁵ Despite these recent achievements, obtaining converged PMFs of antibiotic permeation across porins remains a challenge. Furthermore, since systematic comparisons of augmented US variants are still limited in the literature, finding an optimal US protocol for computing converged PMFs for drug permeation is time-consuming.

In this work, we have compared four methods for computing PMFs of the permeation of fosmidomycin through the OprO porin using a single CV: (i) standalone US,²⁴ (ii) US augmented with Hamiltonian replica exchange with charge-scaling and more specifically with the related REST2 method (US-HREX),^{30,31} (iii) simulated tempering-enhanced umbrella sampling (STeUS),^{33,37} and (iv) replica-exchange umbrella sampling (REUS, also called bias-exchange US, BEUS).²⁹ Whereas OprO forms trimers under native conditions (Figure 1, red cylinders), we here simulated only the monomer to facilitate the computational setups and justified this by the fact

that we focused on finding an efficient sampling method rather than reproducing the native permeation process (Figure 2A).

We identified four key methodological ingredients that were critical for obtaining converged PMFs of the permeation of fosmidomycin through OprO: (i) the use of REUS to enhance sampling during US simulations; (ii) the application of orientational flat-bottomed restraints to maintain one preselected orientation of the elongated solute inside the channel; (iii) the use of cylindrical flat-bottomed restraints to keep the solute in the proximity of the pore axis; and (iv), during the initial constant-velocity pulling of the solute along the channel, the application of position restraints on protein atoms to avoid distortions of pore-lining residues. By combining these ingredients, we obtained PMFs that were converged with 95% confidence intervals below one kilocalorie per mole.

METHODS

Simulation Setup. REUS and US-HREX were carried out with Gromacs³⁸ version 2020.6 built with Open MPI and patched with Plumed version 2.7.2.^{39,40} Standalone US and STeUS were carried out with Gromacs version 2020.4 patched with Plumed 2.7.0. Atomic coordinates of the porin trimers (pdb code 4RJW⁴¹) and fosmidomycin, as well as force field parameters, were kindly provided by Prof. Ulrich Kleinekathöfer.^{26,27} Proteins, lipids, water, and ions were parameterized with the CHARMM36m force field⁴² and fosmidomycin with the CGenFF-based force field generated with the ParamChem server.⁴³ The validation of fosmidomycin parameters is available in ref 26. From the atomic coordinates of the OprO trimers, two monomers have been removed to obtain a monomeric form of the OprO porin. We inserted the monomer into a lipid bilayer of 334 1-palmitoyl-2-oleoyl-*sn*-glycero-3-phosphoethanolamine (POPE) lipids, following Golla et al.,²⁶ with the CHARMM-GUI membrane builder.⁴⁴ Thus, because we focused here on sampling challenges due to antibiotic–protein interactions and not due to antibiotic–lipid interactions, we did not simulate a biologically realistic lipid composition involving lipopolysaccharide lipids. We solvated the system with TIP3P water molecules⁴⁵ and added 14 potassium ions to neutralize the system. For simplicity, the effect of an additional salt was not considered in this study.

Electrostatic interactions were computed with the particle-mesh Ewald method,⁴⁶ using a Fourier grid spacing of 0.12 nm and a real-space cutoff at 1.12 nm. Short-range repulsion and dispersion interactions were described with a Lennard-Jones potential with a cutoff at 1.2 nm and a force-switch modifier set to 1.0 nm. Angles and bonds of water molecules were constrained with SETTLE,⁴⁷ and bonds involving other hydrogen atoms were constrained with LINCS.⁴⁸ Energy minimization was carried out with steepest descent, and equilibration was performed following the six-step protocol provided by CHARMM-GUI.⁴⁴ In brief, the aforementioned equilibration protocol consisted of two 125 ps NVT equilibration simulations, one 125 ps NPT equilibration, and three 500 ps NPT simulations. During equilibration, position restraints were applied on lipid phosphate atoms and to protein and fosmidomycin heavy atoms; restraints were slowly released through the six equilibration steps. Pressure at 1 bar was controlled by the Berendsen barostat ($\tau = 5$ ps) and temperature at 300 K by the Berendsen thermostat ($\tau = 1$ ps).⁴⁹

For production runs, a 4 fs time step was used for standalone US, US-HREX, and REUS, and a 3.5 fs time step was used for STeUS. Using a time step larger than the commonly used 2 fs time step was possible by modeling all hydrogen atoms as virtual sites. The pressure was controlled with the Parrinello–Rahman barostat,⁵⁰ while the temperature was controlled by velocity rescaling.⁵¹

Standalone Umbrella Sampling. To obtain starting conformations of US, we carried out eight 100 ns independent constant-velocity pulling simulations (force constant 1000 kJ mol⁻¹ nm⁻²). We pulled fosmidomycin from the extracellular side (EC) to the periplasmic side (PP) (forward direction) or from PP to EC (reverse direction), each direction with two fosmidomycin orientations as defined in Figure 2C, and we simulated two repetitions for each setup ($2 \times 2 \times 2$ pulling simulations in total). During pulling simulations, we pulled along the *z*-component of the vector connecting (i) the center of mass (COM) of C _{α} atoms close to the cavity and (ii) the COM of the terminal chemical moiety of fosmidomycin in the direction of the movement. For the terminal chemical moieties, we used either a phosphoryl group (PP-to-EC in orientation 1; EC-to-PP in orientation 2) or the amine group (PP-to-EC in orientation 2; EC-to-PP in orientation 1). During pulling simulations, we used three types of restraints that were critical to obtain converged PMFs, as described below. Trajectories from pulling simulations were postprocessed to map each frame onto the CV *z* defined as the *z*-component of the vector connecting the COM of OprO porin C _{α} atoms close to the cavity and the center of mass of the entire fosmidomycin.

After mapping frames onto *z*, we launched 144 umbrella simulations in the range $z \in [-3.4, 3.34]$ nm, corresponding approximately to the *z*-range used by Golla et al.,²⁶ using a force constant of 2000 kJ mol⁻¹ nm⁻² and a simulation time of 30 ns per window. During this equilibration phase, force constants of the restraints on the backbone and side-chain heavy atoms of the protein were reduced to 100 and 10 kJ mol⁻¹ nm⁻², respectively. Final coordinates obtained from the previous step were then used to launch production simulations of 200 ns (Table S1). During production, position restraints on the protein backbone and protein side chains were completely removed. Centers of harmonic potentials used in all US flavors are provided in Figure S1. The choice of umbrella window spacing is described in the Replica-Exchange Umbrella Sampling: REUS section.

All PMFs were computed with wham by Alan Grossfield (“WHAM: the weighted histogram analysis method”, version 2.0.11, http://membrane.urmc.rochester.edu/wordpress/?page_id=126).

Combining Umbrella Sampling with Hamiltonian Replica-Exchange: US-HREX. The CV, number of umbrella windows, spacing between windows, initial configurations, restraints used during production, and US force constant were chosen as during standalone US. To enhance the sampling in higher replicas (corresponding to lower λ values), we scaled charges as depicted in Figure S2A. The protocol used to scale positive and negative charges is shown in Figure S2B.

To identify the λ -range that maintains a stable protein conformation, we ran six simulations for 400 ns with the following λ values: 1, 0.8, 0.6, 0.4, 0.2, 0.1, and 0.05. Simulations with $\lambda = 0.1$ or 0.05 were numerically unstable. However, simulations with $\lambda = 1$ through 0.2 were stable over 400 ns, and visual inspection of trajectories, as well as root-mean-square residue fluctuations, did not indicate protein

unfolding. For production, we ran 24 λ -replicas for each of our 144 umbrella windows. In order to obtain $\sim 19\%$ of exchange acceptance between the 24 replicas, we scaled positive charges from $\lambda = 1$ to 0.793 in steps of 0.009. Each umbrella window was simulated for 9 ns, leading with 24 replicas to an overall simulation time of 216 ns per window (Table S1). Thus, the total simulation time per US window was similar to the 200 ns simulation time used for the other US flavors.

Combining Umbrella Sampling with Simulated Tempering: STeUS. The CV z , number of umbrella windows, initial configurations, restraints used during production, total simulation time, and US force constant were chosen as those during standalone US (Table S1). Simulated tempering was carried out with temperatures ranging from 300 to 348 K in steps of 4 K. We chose the initial temperature weights following Park et al.,⁵² which involves simulated annealing simulation from the lowest to the highest temperature. Accordingly, the weights were chosen as

$$g_{n+1} - g_n \approx (\beta_{n+1} - \beta_n) \frac{E_n + E_{n+1}}{2} \quad (1)$$

where g_n is the weight of the state with temperature T_n , $\beta_n = 1/k_B T_n$ is the respective inverse temperature, and E_n is the average potential energy for temperature state T_n . To obtain the E_n values, we carried out a simulated annealing simulation for the umbrella window restrained to $z = 0$ nm, for which the temperature was increased from 300 to 348 K, with 2 ns per temperature state and 100 ps for each heating step over a total simulation time of 27.2 ns. With this protocol, we obtained the following weights from g_0 through g_{12} : 0, 4370.5, 8600.3, 12 694.8, 16 659.9, 20 500.2, 24 220.5, 27 826.5, 31 322.1, 34 711.3, 37 999.4, 41 189.1, and 44 284.0.

To further optimize the weights, we carried out a simulated tempering simulation for an umbrella window corresponding to $z = 0$ nm with the previously determined weights, with an exchange attempt every 100 steps and using the Wang–Landau algorithm over a total simulation time of 43 ns. This simulation was used to determine the final weights used for production: 0, 4361.5, 8577.3, 12 657.8, 16 617.9, 20 459.2, 24 166.5, 27 768.5, 31 265.1, 34 644.3, 37 926.4, 41 114.1, and 44 206.0. Finally, each of the 144 umbrella windows has been run with simulated tempering using final weights determined as explained above, with exchange attempt every 100 steps. During final STeUS simulations, the weights were stable and all states were visited with similar occupancies (Figure S3). Only simulation frames at the ground temperature T_0 were used to collect the US histograms and hence to compute the PMF.

Replica-Exchange Umbrella Sampling: REUS. The CV z , number of umbrella windows, initial configurations, restraints used during production, total simulation time, and US force constant were chosen as during standalone US (Table S1). To choose the spacing between the 144 umbrella windows along z , we ran a series of 60 ps simulations and optimized the spacing to reach an acceptance probability for exchanges between neighboring windows in the range of 0.25–0.47%. During our optimization process, we assumed a linear relation between the z -spacing and the rejection probability within the tested range of window spacings (Figure S4). Then, we selected a z -spacing between windows with an expected exchange rejection probability of 0.64%. Because running 144 umbrella windows in parallel would require the simultaneous allocation of many compute nodes, we grouped our umbrella

windows into 11 subsets along the z -range, and we allowed exchanges only within the subsets. To guarantee a good overlap between umbrella windows at the ends of the subsets, neighboring subsets overlapped by two umbrella windows (Figures S5 and S6). Because the constriction region of OprO at $[-1$ and $1]$ nm was subject to increased sampling problems due to extensive contacts between the porin and fosmidomycin, we used more replicas for the subset close to this region. Hence, the subset centered at $z = 0$ nm was composed of 24 windows, while all other subsets were composed of 16 windows except for the two subsets including the z -range extrema, which were composed of only eight windows. The average exchange probabilities of our production REUS were consistent with our optimization procedure, i.e., nearly all exchange probabilities were within the $[0.25\%, 0.47\%]$ range with only a few exceptions (Figures S5 and S6).

Restraints Used during Initial Pulling and during Umbrella Sampling. During the initial pulling simulation (steered MD) and during US, we applied an orientational flat-bottomed restraint as well as a cylindrical flat-bottomed restraint to the fosmidomycin. During the initial pulling and equilibration only, we applied in addition position restraints on protein atoms, as described and rationalized in the following sections.

Flat-Bottomed Orientation Restraints. The angle between the vector connecting the two ends of the drug and the z -axis was restrained with a flat-bottomed potential within $[-45^\circ, 45^\circ]$, using a force constant of $7878 \text{ kJ mol}^{-1} \text{ rad}^{-2}$ outside of this interval. The angle restraints were used to maintain fosmidomycin either in orientation 1 or in orientation 2 as defined in Figure 2C. The orientation restraint was strictly required to obtain converged PMFs because sampling of an orientational flip is extremely rare in the narrow pore (if not impossible). As such, we computed two PMFs, one for each orientation, which may be combined a posteriori if needed.

Flat-Bottomed Cylindrical Restraint along the Pore Axis. In addition, we applied a flat-bottomed potential to restrain the antibiotic within a cylinder of radius 1 nm centered on the COM of C_α atoms close to the cavity with a force constant of $1000 \text{ kJ mol}^{-1} \text{ nm}^{-2}$ acting outside of the cylinder in the direction of the cylinder axis (Figure 2B). The cylindrical flat-bottomed potential ensured that the solute would not “miss” the entrance to the pore. Since the pore vestibules have diameters of approximately 16 Å or less, while the constriction regions are even narrower, the flat-bottomed region was large enough to ensure that the solute did not feel the potential if located in the constriction regions or in the vestibules. Furthermore, the cylindrical flat-bottomed potentials serve to obtain a bulk state with well-defined entropy and free energy. Although not considered in this study, such a well-defined bulk free energy would be needed to compute the overall permeability of a membrane with a given lateral concentration of porins.

Protein Restraints during Initial Steered MD. To mitigate nonequilibrium effects during pulling simulations, we used position restraints on heavy atoms of the protein backbone and side chains with force constants of 1000 and $100 \text{ kJ mol}^{-1} \text{ nm}^{-2}$, respectively. These restraints excluded the possibility that the protein would be distorted during pulling simulations, which would lead to hysteresis problems, i.e., to different PMFs obtained from pulling along PP-to-EC and for EC-to-PP directions. These restraints were gradually decreased

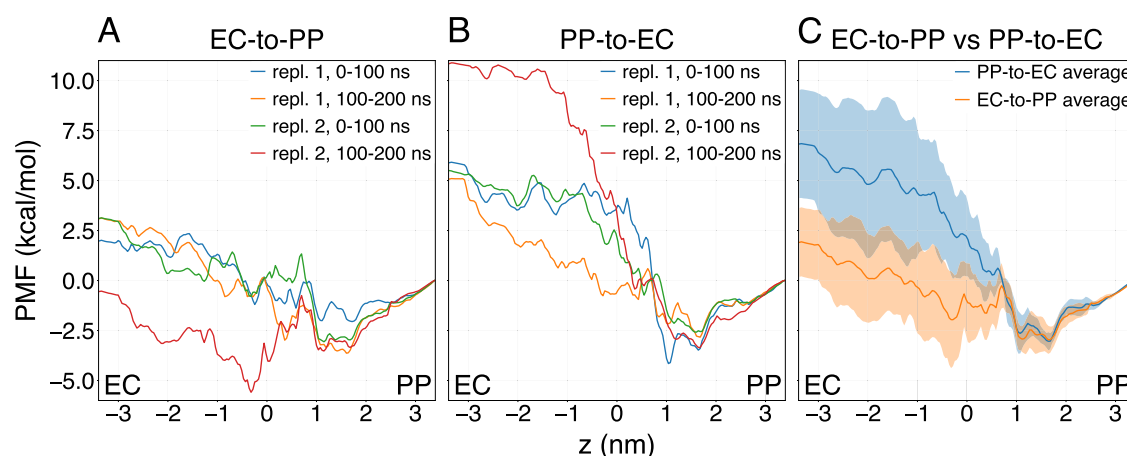


Figure 3. PMFs of fosmidomycin permeation in orientation 1 with standalone US obtained after (A) EC-to-PP pulling or (B) PP-to-EC pulling. Two independent pulling simulation replicates were carried out for each direction and used to obtain initial frames for US. For each replicate, umbrella windows were binned into two time blocks of 0–100 and 100–200 ns, yielding a total of four PMFs for each permeation direction (blue, orange, red, and red lines). (C) Average PMF for each direction. Confidence intervals (shaded areas) represent two standard errors. Evidently, PMFs from the standalone US are poorly converged and subject to major hysteresis problems.

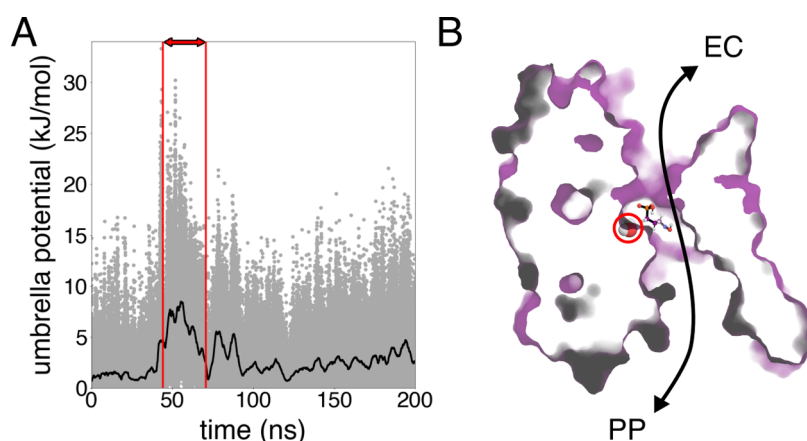


Figure 4. On the influence of water on poor convergence during standalone US. (A) Bias potential energy of umbrella window centered at $z = -0.007$ nm vs simulation time (gray dots) and smoothed with the scipy module `uniform_filter1d`⁵⁶⁶ with a filter size of 5000 points (black line). (B) Representative snapshot during simulation time between 45 and 71 ns (red box in panel A). The water molecule trapped between fosmidomycin (represented as balls and sticks) and porin (represented as a surface) is highlighted with a red circle. The double-headed black arrow sketches the OprO lumen.

during equilibration (see above) and fully removed during production simulations.

RESULTS

Permeation of Fosmidomycin in Orientation 1 with Standalone US. In the work from Golla et al.,²⁶ PMFs of the permeation of fosmidomycin through OprO computed with standalone US exhibited hysteresis effects. To test how REUS, STeUS, and US-HREX improve the PMFs relative to standalone US, we first computed reference PMFs with standalone US. As CV, we used the z -component of the distance vector between the center of mass of OprO C_α atoms close to the porin lumen (referred to as pCOM) and the center of mass of the fosmidomycin phosphoryl group and amine group (referred to as fCOM) (Figure 2B). Henceforth, we refer to this CV as z . We reduced the accessible configurational space by (i) restraining the orientation of the antibiotic relative to the z -axis within $\pm 45^\circ$ (Figure 2C) and (ii) by applying a flat-bottomed potential restraining the distance between the pCOM and the fCOM projected onto the xy -plane below 1 nm

(Figure 2B; see Methods). By using an orientational restraint, fosmidomycin could enter the porin from the EC by presenting either its amine group first (orientation 1) or its phosphoryl group first (orientation 2) (Figure 2C). For standalone US, we investigated only orientation 1.

Because the free energy is a state function, PMFs computed with umbrella sampling should not depend on the path taken by the initial pulling simulations^{53,54} used to generate the initial configurations. A sensitive test for the convergence of PMFs computed with umbrella sampling is to compare PMFs obtained with initial configurations generated from “forward” and “reverse” pulling simulations, here corresponding to initial pulling in the EC-to-PP and PP-to-EC directions, respectively. Figure 3A,B presents PMFs obtained from EC-to-PP or PP-to-EC pulling simulations, where the PMFs were defined to zero at the largest z -position. Each panel shows four PMFs based on two independent pulling simulations (rep 1 and rep 2), while each 200 ns US window was furthermore split into two time blocks of 0–100 and 100–200 ns. The average PMFs for EC-to-PP and PP-to-EC directions are shown in Figure 3C

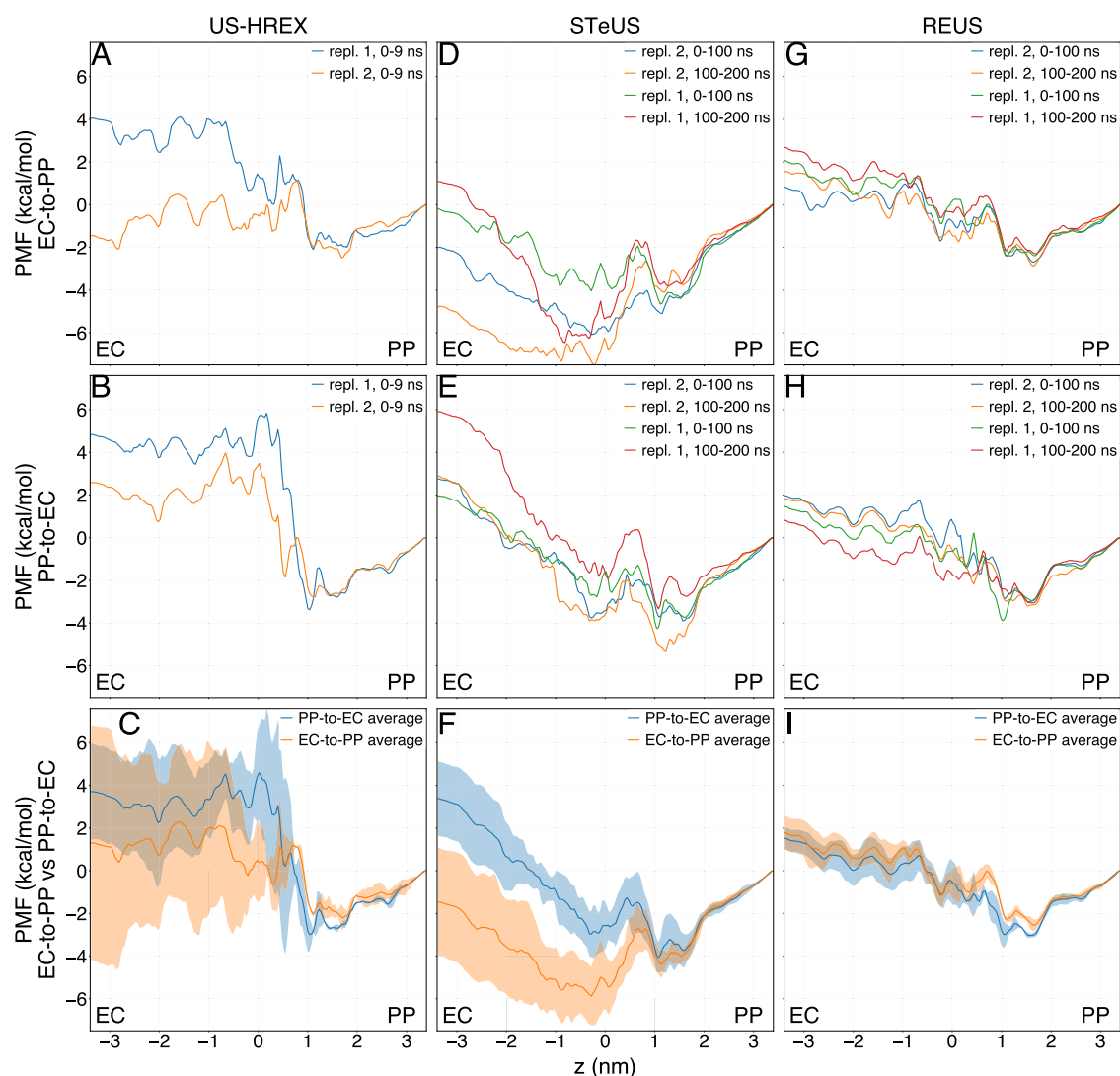


Figure 5. PMFs of fosmidomycin permeation in orientation 1 obtained with US-HREX (A, C), STeUS (D, F), or REUS (G, I). EC-to-PP (A, D, G) and PP-to-EC PMFs (B, E, H) were computed with initial conformations obtained from EC-to-PP and PP-to-EC pulling simulations, respectively. For each EC-to-PP and PP-to-EC setup, two independent pulling simulations were carried out: replicates 1 and 2. For STeUS and REUS, umbrella windows were binned into time blocks 0–100 ns and 100–200 ns, respectively. (C, F, I) Averages of EC-to-PP (orange) and PP-to-EC (blue) PMFs by combining all respective umbrella windows. Confidence intervals (shaded areas) estimated from independent PMFs represent two standard errors.

together with two standard errors as shaded areas, revealing 95% confidence intervals up to $7.5 \text{ kcal mol}^{-1}$ or up to $5.0 \text{ kcal mol}^{-1}$ for the EC-to-PP or PP-to-EC directions, respectively, demonstrating major statistical uncertainties. In addition, the free-energy difference between the PP and EC end points strongly differs between the EC-to-PP and PP-to-EC PMFs, demonstrating a major hysteresis problem. Notably, without the use of restraints during US and initial pulling (see [Methods](#)), as done previously,⁵⁵ these hysteresis problems would likely be even more pronounced.

To shed light on the molecular interactions underlying the hysteresis, we inspected the umbrella potential energy over time in different umbrella windows to detect a high variation of the bias potential. We observed a bias potential peak in the umbrella window centered at $z = -0.007 \text{ nm}$ (Figure 4A); this peak correlates with the presence of a water molecule trapped between fosmidomycin and the protein (Figure 4B, red circle). Thus, solvent degrees of freedom likely contributed to the observed hysteresis effects. In line with the work from Golla et

al., our results confirm that using z as a collective variable with standalone umbrella sampling is not sufficient to sample all relevant degrees of freedom involved in fosmidomycin permeation through OprO using 200 ns per US window, even in the presence of several restraints.

Comparison of US Flavors for Fosmidomycin in Orientation 1: US-HREX, STeUS, and REUS. To overcome the sampling and hysteresis problems with standalone US (previous paragraph), we tested three improved US flavors, namely, US-HREX, STeUS, and REUS. To apply US-HREX in practice, it is critical to understand the molecular interactions underlying the free-energy barriers along the orthogonal degrees of freedom. Here, because cationic residues inside the OprO lumen strongly interact with fosmidomycin,²⁶ we chose to scale positive charges of the porin and negative charges within the phosphoryl group of fosmidomycin by the λ -parameter along 24 λ -replicas per US window (see [Methods](#) for details).

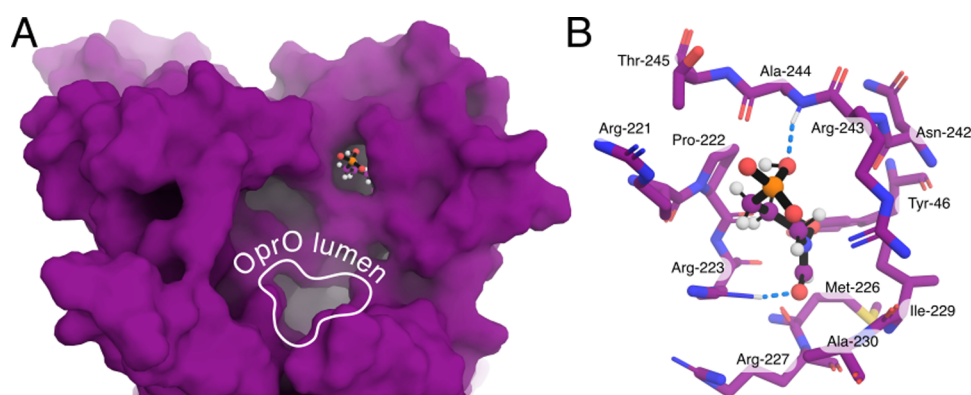


Figure 6. (A) Snapshot of the umbrella window centered at $z = -1.63$ nm from STeUS, revealing fosmidomycin trapped in a pocket near the EC entrance. OprO is represented as a purple surface, and fosmidomycin is represented as balls and sticks. (B) Focus on fosmidomycin and protein residues of the pocket. Blue dotted lines indicate fosmidomycin–protein hydrogen bonds.

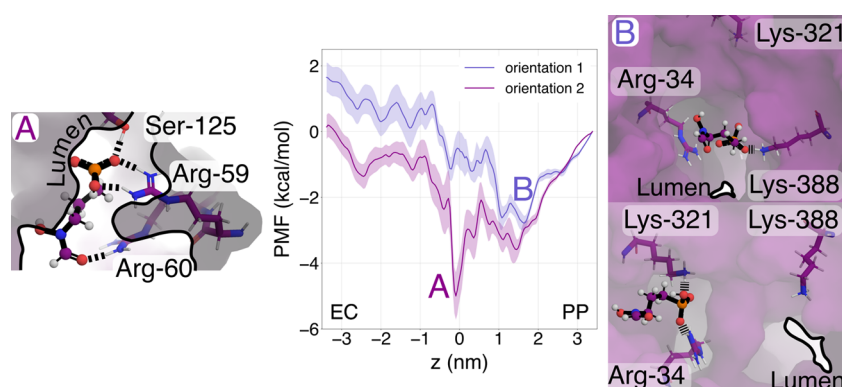


Figure 7. Averaged PMFs of fosmidomycin permeation in orientation 1 (dark blue) or orientation 2 (magenta) computed with REUS, after combining EC-to-PP and PP-to-EC calculations. Example simulation snapshots of the conformation of the free-energy minima for orientations 1 and 2 are depicted in panels B and A, respectively. Confidence intervals (shaded areas) represent two standard errors.

Increasing the temperature is another means to improve sampling. This principle is exploited in the simulated tempering framework, where a Metropolis criterion is used to accept or reject steps along a predefined temperature ladder within a single simulation. In higher-temperature states, the probability to cross enthalpic barriers together with exchanges with low-temperature states will improve configurational sampling at all temperatures, including the base temperature. Combining simulated tempering with umbrella sampling in STeUS has been highly successful during PMF calculations for drug permeation across a lipid membrane.³³ In this study, simulated tempering was applied in each umbrella window with temperatures ranging from 300 to 348 K with 4 K-steps, and only data acquired at the base temperature was used to compute the PMFs (see [Methods](#) for details).

REUS (also referred to as bias-exchange US) exploits the fact that neighboring umbrella windows can explore different regions of phase space and, therefore, by exchanging configurations between windows according to a Metropolis criterion,⁵⁷ improved sampling of relevant degrees of freedom orthogonal to the CV is expected. In REUS, it is common practice to permit configuration exchanges along the whole CV space. In this study, in contrast, we permitted exchanges only between windows within subsets of z to reduce the amount of computational resources needed simultaneously (see [Methods](#)).

PMFs of the fosmidomycin permeation through OprO obtained with the three aforementioned methods are shown in

[Figure 5](#). The PMFs obtained with US-HREX exhibit a steep increase at $z \approx 1$ nm, suggesting that these PMFs suffer from hysteresis problems ([Figure 5A,B](#)). In addition, the EC-to-PP and PP-to-EC PMFs from US-HREX strongly differ within the region $|z| < 1$ nm, and the averaged PMFs exhibit large statistical errors ([Figure 5C](#)). Hence, US-HREX hardly improved the sampling relative to standalone US. Compared to the PMFs from US-HREX, the PMFs from STeUS are slightly more converged, as is evident from the slightly reduced uncertainties ([Figure 5F](#)) and from the absence of a spurious increase at $z \approx 1$ nm ([Figure 5D,E](#)). Nevertheless, the major statistical uncertainties remain with STeUS as well as a major hysteresis between EC-to-PP and PP-to-EC directions.

To understand why PMFs of the permeation of fosmidomycin through OprO computed with STeUS display hysteresis problems, we visually inspect the trajectories. Accordingly, we noticed that fosmidomycin has been trapped in a pocket at the EC entrance of OprO in the umbrella window centered at $z = -1.63$ nm ([Figure 6](#)). The transition toward this pocket occurred after ~ 100 ns, while fosmidomycin remained in this pocket for the remaining 100 ns, irrespective of a uniform coverage of all temperature states. Hence, simulated tempering did not help fosmidomycin escape from this pocket within the simulation time. To further test the stability of this unexpected state, we ran three free simulations of 100 ns, each starting from configurations extracted at $t = 130, 160,$ and 200 ns of this US window. Fosmidomycin did not escape the pocket in any of these simulations. Besides the

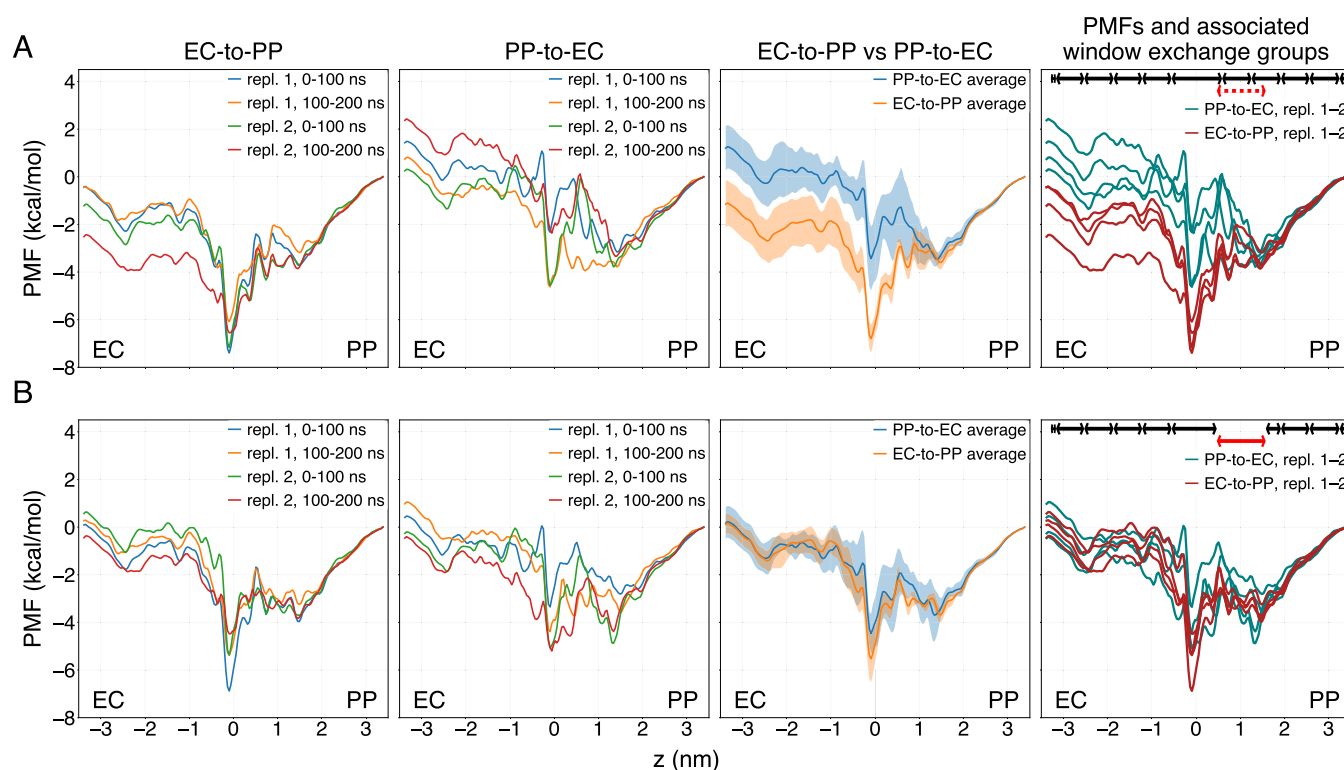


Figure 8. PMFs of fosmidomycin permeation in orientation 2 with REUS. (A) PMFs of the permeation process with the suboptimal choice of window subsets within which exchanges are allowed. EC-to-PP and PP-to-EC PMFs refer to REUS setups started with initial conformations obtained from EC-to-PP and PP-to-EC pulling simulations, respectively (two left columns; see panel headings). For each setup, two independent pulling simulations were carried out: replicates 1 and 2. Umbrella windows were binned into time blocks 0–100 ns and 100–200 ns, yielding two PMFs for each direction and orientation (see legends). Third column: average EC-to-PP (orange) and PP-to-EC (blue) PMFs, with confidence intervals representing two standard errors. Right column: US windows within z -subsets delimited by the dark arrows were carried out in parallel and, therefore, were allowed to exchange configurations. The region within the red-dotted arrow shows a high discrepancy between EC-to-PP and PP-to-EC PMFs, indicative of limited sampling. (B) PMFs of the permeation process with an optimized choice of window subsets within which exchanges are allowed. Descriptions of each column are identical to panel (A), except that data from a new REUS batch in the region $z = [0.5, 1.5]$ nm (solid red arrow region in the fourth column) were used to obtain the PMFs.

population of this unexpected state that does not contribute to successful permeation, we furthermore observed strongly increased flexibility of protein loops relative to the other US flavors as a consequence of populations of higher-temperature states during simulated tempering. These results suggest that, for simulating permeation across OprO, the use of simulated tempering increases the risks of (i) populating nonproductive conformation and (ii) of partly unfolding the protein.

In sharp contrast to the PMFs obtained with US-HREX or STeUS, PMFs obtained with REUS were highly converged and exhibited virtually no hysteresis problems (Figure 5G–I). Along the complete CV, the EC-to-PP and PP-to-EC PMFs revealed excellent agreement with a maximum deviation of ~ 1 kcal/mol (Figure 5I), while the 95% confidence intervals were smaller or close to 1 kcal/mol (Figure 5I, shaded areas), by far lower as compared to the confidence intervals obtained with US-HREX, STeUS, or standalone US (Figures 3C and 5C,F). Taken together, among the four US flavors considered in this study, REUS provides by far the best-converged PMFs of fosmidomycin permeation across OprO.

The agreement of EC-to-PP PMFs with PP-to-EC PMFs obtained from REUS justifies the averaging of these PMFs to further reduce the statistical uncertainties. By averaging all EC-to-PP and PP-to-EC PMFs computed with REUS, we obtained PMFs for fosmidomycin permeation in orientation 1 with 95% confidence intervals of approximately 0.5 kcal/mol (Figure 7,

blue curve). The free-energy minimum of the PMF in orientation 1 at $z = 1.6$ nm corresponds to a wider region of the pore, where fosmidomycin may adopt different sets of interactions with Arg³⁴, Lys³²¹, or Lys³⁸⁸ (Figure 7, right panel).

Permeation of Fosmidomycin in Orientation 2 with REUS. The PMFs discussed in the sections above correspond to orientation 1 of fosmidomycin, with the phosphate moiety pointing toward the extracellular side (Figure 2C). We proceeded to test whether REUS likewise provides converged PMFs for fosmidomycin in orientation 2, initially using the same computational effort as used for orientation 1. However, unlike the PMFs for orientation 1 that were largely overlapping among the EC-to-PP and PP-to-EC directions (Figure 5G–I), the PMFs for orientation 2 overlapped only in the region between 0.5 and 3.5 nm, mostly owing to hysteresis problems in the range $z = [0.5, 1.5]$ nm (Figure 8A). In our implementation of REUS, exchanges between neighboring US windows were allowed only within subsets of the z -space (Figure 8A, right panel, black segments). Therefore, we hypothesized that sampling could be improved in regions of z -space that exhibit the largest discrepancies between EC-to-PP and PP-to-EC PMFs by increasing the number of windows that may exchange configurations.

By overlaying all PMFs, we observed that the shape of the EC-to-PP and PP-to-EC PMFs largely agreed except in the region $z \in [0.45, 1.54]$ nm (Figure 8A, last column). Thus, we

carried out an additional batch of 24 REUS windows within this z -region for each replicate (red bar in Figure 8B, fourth column), and we allowed for exchanges between all 24 windows within this batch. Upon replacing the previous US windows of this z -range with the new batch of simulation data, we obtained PMFs with a favorable agreement between the EC-to-PP and PP-to-EC directions, hence revealing the absence of hysteresis problems (Figure 8B). The 95% confidence intervals were ≤ 1.5 kcal/mol throughout the CV for both PP-to-EC and EC-to-PP PMFs (Figure 8B, third column). Hence, we obtained well-converged PMFs also in orientation 2 by (i) identifying the undersampled region via comparing PMFs from forward and reverse pulling and (ii) enabling exchanges over the complete undersampled regions.

By averaging all EC-to-PP and PP-to-EC PMF replicates in Figure 8B, we obtained the PMF with 95% confidence intervals below 1 kcal/mol for orientation 2 (Figure 7, magenta curve). The PMF for orientation 2 reveals a marked free-energy minimum at the channel center at $z = -0.1$ nm, where fosmidomycin forms simultaneous hydrogen bonds with Arg⁵⁹, Arg⁶⁰, and Ser¹²⁵ (Figure 7, left panel).

DISCUSSION

We compared four different US flavors for studying the permeation of fosmidomycin through the OprO porin using only a single CV: standalone US, REUS, STeUS, and US-HREX. Among these methods, REUS revealed by far the best-converged PMFs. For a given fosmidomycin orientation, using a total simulation time of approximately 65 μ s, REUS achieved PMFs that were converged with 95% confidence intervals (two standard errors) well below one kilocalorie per mole. Although the computational effort for obtaining the converged PMF is considerable, we expect that with the ever-increasing computer power simulations as presented here may soon become routine for studying antibiotic uptake by outer membrane porins.

Our key assessment of convergence was given by the comparison of PMFs obtained after constant-velocity pulling simulations in forward or reverse directions, here corresponding to PP-to-EC or EC-to-PP directions, respectively. Because PMF calculations frequently suffer from hysteresis problems, comparing PMFs obtained after forward and reverse pulling provides a highly sensitive test for convergence.^{58–60} In addition, for each pulling direction (PP-to-EC or EC-to-PP), we computed PMFs from two independent sets of US windows initiated from two independent pulling simulations. Comparing the latter PMFs provides an additional quality test but may not reveal hysteresis problems that are, in our experience, a major matter of concern during US simulations of biomolecules. An alternative strategy for estimating statistical errors may be given by splitting the US windows into time blocks, followed by a comparison of the PMFs obtained from each time block. However, because autocorrelation times are typically unknown and may exceed the simulation time of US windows, the PMFs obtained from time blocks may not be independent, and statistical errors may be severely underestimated. Hence, we suggest that the comparison of PMFs obtained after pulling in the forward and reverse directions should become routine when reporting PMFs from US simulations of biomolecular simulations.

Poor conformational sampling is a consequence of long autocorrelation times, owing to long-living conformational arrangements of solute, protein, and channel-bound water molecules. Since both HREX and simulated tempering have

been used successfully to enhance the conformational sampling of protein or membrane systems,^{33,61–63} we anticipated that augmenting US with HREX (US-HREX) or with simulated tempering (STeUS) would accelerate the converge of PMF calculations of fosmidomycin permeation. However, US-HREX and STeUS provided only a small sampling benefit (if any) as compared to standalone US. The benefit of US-HREX is furthermore reduced owing to the requirement of simulating parallel replicas of each US window. Moreover, the use of US-HREX is complicated by the fact it requires the selection of a set of interactions to be scaled along the λ -variable, which is *a priori* far from obvious. In our implementation of US-HREX, we scaled the charges of fosmidomycin and cationic residues with the aim of reducing the lifetime of salt bridges at higher λ -states and, thereby, to reduce autocorrelation times. Such a choice may provide room for further optimization, for instance, by restricting the scaling to cationic residues along the pore lumen or, considering that the OprO pore poses a steric hindrance against permeation,⁶⁴ by scaling Lennard-Jones parameters. However, since US-HREX was hardly successful and computationally expensive, we did not further optimize the selection of scaled interactions.

We recently observed at least 5-fold enhanced sampling by STeUS relative to standalone US for drug permeation across a lipid membrane.³³ For fosmidomycin permeation across OprO, in contrast, STeUS provided only a small benefit, suggesting that higher temperatures reduced autocorrelation times only moderately. A disadvantage of the simulating tempering simulations as observed here may be an increased risk of visiting conformations that do not contribute to the permeation process (Figure 4) or a risk of perturbing the protein structure at higher temperatures. Similar risks may not apply in disordered systems such as lipid membranes. Hence, additional simulations will be required to clarify which systems benefit from simulated tempering during US.

According to our REUS protocol, we split our CV space into several subsets of 8–24 neighboring US windows, allowing exchanges of configurations only within a subset. Compared to more common REUS setups that allow exchanges among all windows within a single simulation batch, our protocol greatly reduces the number of simultaneously allocated compute nodes, hence allowing the efficient use of compute clusters without longer waiting times and the use of REUS simulations on commodity clusters. Furthermore, such a protocol readily allows dedicating more resources and longer simulation times to CV regions that are critical for sampling.

A critical requirement for obtaining converged PMFs with REUS was the use of several types of restraints. (i) We restrained the orientation of fosmidomycin relative to the z -axis within $\pm 45^\circ$. The orientational restraint avoids long autocorrelation times owing to the slow conformational sampling of the fosmidomycin orientation in the pore lumen. Indeed, during an early stage of this project, we obtained poorly converging PMFs in REUS simulations without orientation restraints. (ii) A flat-bottomed cylindrical restraint acting in the lateral direction kept fosmidomycin near the pore axis. Such a restraint excluded that the solute diffuses laterally in the complete xy -plane of the simulation box, which would lead to sampling problems in US windows near the pore entrance. (iii) During initial constant-velocity pulling simulations of fosmidomycin across the pore, it was critical to restrain the positions of protein atoms. Without such restraints, the protein structure may be perturbed because the steered

fosmidomycin molecule may drag protein residues or distort geometric constriction sites. Because the equilibration time of US windows is typically insufficient to mitigate such structural perturbations, perturbations would lead to undesired hysteresis problems.

Since we focused in this study on sampling challenges for fosmidomycin positions along the pore lumen and to reduce the computational cost, we used a relatively small simulation system (Figure 2A) and restricted the US simulations to a range of approximately $z \in [-3.4, 3.4]$ nm. At the end points of the PMFs, fosmidomycin had a distance of ~ 1 nm from OprO, where fosmidomycin was still interacting with OprO by long-ranged interactions, as reflected by the remaining slopes of the PMFs at $z \approx \pm 3.4$ nm (Figure 7, middle panel). To compute absolute binding free energies and permeabilities for antibiotics in future studies, it will be required to use larger simulation systems and extend the antibiotic permeation process into the bulk solvent, where the PMFs would reach a plateau.

Quantitative predictions of membrane permeability for antibiotics involve several additional challenges, which were not addressed in this study. Antibiotic permeation may be regulated by large-scale gating transitions of flexible loops,^{23,35} whose conformational ensembles may depend on single amino acid substitutions⁶⁵ or on the presence of an antibiotic. Since ensembles of flexible loops are hard to converge within individual umbrella windows, additional computational developments may be required to obtain converged PMFs in the presence of flexible loops. The outer membrane of Gram-negative bacteria is highly complex and decorated with large lipopolysaccharide moieties, which extend by several nanometers into extracellular space. Thus, in the biological context, interactions with lipids may influence antibiotic permeability even if the permeation proceeds across the porin and not across the lipid bilayer. Obtaining the permeability requires, apart from the PMF, also the calculation of the position-dependent diffusion coefficient.⁶⁶ Because the anionic fosmidomycin binds to the cationic OprO lumen, as shown by the free-energy minima along the PMF (Figure 7), fosmidomycin permeation may involve competitive binding with other anionic species such as phosphate ions, which were not simulated here. Furthermore, apart from overcoming sampling challenges addressed here, accurate permeability predictions rely on accurate force fields. The uncertainties of computed drug binding free energies owing to limitations of modern force fields are on the order of only 1 kcal/mol;⁶⁷ however, considering that salt bridges are subject to uncertainty in biomolecular simulations,⁶⁸ careful force field validations will be critical for obtaining accurate PMFs for the permeation of ionic solutes such as fosmidomycin.

CONCLUSIONS

We compared four different US flavors used to compute the PMF of permeation of the antibiotic fosmidomycin across the outer membrane porin OprO: standalone US, US augmented with HREX (US-HREX) or with simulated tempering (STeUS), and REUS. In contrast to PMFs obtained with standalone US, US-HREX, or STeUS, the PMFs obtained with REUS were well converged as shown by the absence of hysteresis between PMF calculations carried out in forward and reverse directions and by 95% confidence intervals below one kilocalorie per mole. The convergence of PMFs obtained with REUS relied on the use of several geometric restraints

that helped the simulations to circumvent long autocorrelation times and to avoid structural perturbations during initial pulling simulations. We anticipate that the systematic comparison of US flavors, as well as the protocol for obtaining converged PMFs of OprO permeation, will be useful for studying antibiotic uptake over various porins in future studies.

ASSOCIATED CONTENT

Data Availability Statement

The GROMACS molecular simulation package and PLUMED plugin are free of charge. Molecular figures were generated with PyMOL, an open-source molecular visualization software. Data are available upon request.

Supporting Information

The Supporting Information is available free of charge at <https://pubs.acs.org/doi/10.1021/acs.jcim.3c00880>.

Summary of US simulations carried out for this study; umbrella window centers for EC-to-PP and PP-to-EC; Hamiltonian replica-exchange protocol; temperature state probabilities versus time for window $z = 0$ nm; protocol for optimizing the distance between neighboring umbrella windows for REUS; average exchange probabilities between umbrella windows; and umbrella window overlap (PDF)

AUTHOR INFORMATION

Corresponding Author

Jochen S. Hub – *Theoretical Physics and Center for Biophysics, Saarland University, Saarbrücken 66123, Germany*; orcid.org/0000-0001-7716-1767; Phone: +49 (0)681 302-2740; Email: jochen.hub@uni-saarland.de; Fax: +49 (0)681 302-6604

Author

Jeremy Lapierre – *Theoretical Physics and Center for Biophysics, Saarland University, Saarbrücken 66123, Germany*; orcid.org/0000-0003-2265-290X

Complete contact information is available at: <https://pubs.acs.org/10.1021/acs.jcim.3c00880>

Notes

The authors declare no competing financial interest.

ACKNOWLEDGMENTS

The authors thank Ulrich Kleinekathöfer and Vinaya Kumar Golla for fruitful discussions, for pointing out the challenges of converging PMF calculations of porin permeation, and for kindly sharing the simulation systems and force field parameters of OprO and fosmidomycin. This study was supported by the Deutsche Forschungsgemeinschaft (DFG, German Research Foundation) via grants SFB 860/A16 and INST 256/539-1.

REFERENCES

- (1) Cross, A.; Allen, J. R.; Burke, J.; Ducle, G.; Harris, A.; John, J.; Johnson, D.; Lew, M.; MacMillan, B.; Meers, P.; et al. Nosocomial infections due to *Pseudomonas aeruginosa*: review of recent trends. *Rev. Infect. Dis* 1983, 5, S837–S845, DOI: [10.1093/clinids/5.Supplement_5.S837](https://doi.org/10.1093/clinids/5.Supplement_5.S837).
- (2) Fazzeli, H.; Akbari, R.; Moghim, S.; Narimani, T.; Arabestani, M. R.; Ghodoussi, A. R. *Pseudomonas aeruginosa* infections in patients,

- hospital means, and personnel's specimens. *J. Res. Med. Sci.* **2012**, *17*, 332.
- (3) Qin, S.; Xiao, W.; Zhou, C.; Pu, Q.; Deng, X.; Lan, L.; Liang, H.; Song, X.; Wu, M. *Pseudomonas aeruginosa*: pathogenesis, virulence factors, antibiotic resistance, interaction with host, technology advances and emerging therapeutics. *Signal Transduction Targeted Ther.* **2022**, *7*, 1–27.
- (4) Daikos, G. L.; da Cunha, C. A.; Rossolini, G. M.; Stone, G. G.; Baillon-Plot, N.; Tawadrous, M.; Irani, P. Review of Ceftazidime-Avibactam for the Treatment of Infections Caused by *Pseudomonas aeruginosa*. *Antibiotics* **2021**, *10*, No. 1126, DOI: [10.3390/antibiotics10091126](https://doi.org/10.3390/antibiotics10091126).
- (5) Benz, R. Permeation of hydrophilic solutes through mitochondrial outer membranes: review on mitochondrial porins. *Biochim. Biophys. Acta, Rev. Biomembr.* **1994**, *1197*, 167–196.
- (6) Nikaido, H. Molecular basis of bacterial outer membrane permeability revisited. *Microbiol. Mol. Biol. Rev.* **2003**, *67*, 593–656.
- (7) Piselli, C.; Benz, R. Fosmidomycin transport through the phosphate-specific porins OprO and OprP of *Pseudomonas aeruginosa*. *Mol. Microbiol.* **2021**, *116*, 97–108.
- (8) Zgurskaya, H. I.; Rybenkov, V. V. Permeability Barriers of Gram-negative Pathogens. *Ann. N. Y. Acad. Sci.* **2020**, *1459*, 5–18.
- (9) Lambert, P. A. Cellular impermeability and uptake of biocides and antibiotics in Gram-positive bacteria and mycobacteria. *J. Appl. Microbiol.* **2002**, *92*, 46S–54S.
- (10) Gellatly, S. L.; Hancock, R. E. *Pseudomonas aeruginosa*: new insights into pathogenesis and host defenses. *Pathog. Dis.* **2013**, *67*, 159–173.
- (11) Chevalier, S.; Bouffartigues, E.; Bodilis, J.; Maillot, O.; Lesouhaitier, O.; Feuilloley, M. G.; Orange, N.; Dufour, A.; Cornelis, P. Structure, function and regulation of *Pseudomonas aeruginosa* porins. *FEMS Microbiol. Rev.* **2017**, *41*, 698–722.
- (12) Ude, J.; Tripathi, V.; Buyck, J. M.; Söderholm, S.; Cunrath, O.; Fanous, J.; Claudi, B.; Egli, A.; Schleberger, C.; Hiller, S.; Bumann, D. Outer Membrane Permeability: Antimicrobials and Diverse Nutrients Bypass Porins in *Pseudomonas Aeruginosa*. *Proc. Natl. Acad. Sci. U.S.A.* **2021**, *118*, No. e2107644118.
- (13) Vergalli, J.; Bodrenko, I. V.; Masi, M.; Moynié, L.; Acosta-Gutiérrez, S.; Naismith, J. H.; Davin-Regli, A.; Ceccarelli, M.; van den Berg, B.; Winterhalter, M.; Pagès, J. M. Porins and small-molecule translocation across the outer membrane of Gram-negative bacteria. *Nat. Rev. Microbiol.* **2020**, *18*, 164–176.
- (14) Prajapati, J. D.; Kleinekathöfer, U.; Winterhalter, M. How to Enter a Bacterium: Bacterial Porins and the Permeation of Antibiotics. *Chem. Rev.* **2021**, *121*, 5158–5192.
- (15) Hoshino, Y.; Gaucher, E. A. On the Origin of Isoprenoid Biosynthesis. *Mol. Biol. Evol.* **2018**, *35*, 2185–2197.
- (16) Ceccarelli, M.; Danelon, C.; Laio, A.; Parrinello, M. Microscopic Mechanism of Antibiotics Translocation through a Porin. *Biophys. J.* **2004**, *87*, 58–64.
- (17) Danelon, C.; Nestorovich, E. M.; Winterhalter, M.; Ceccarelli, M.; Bezrukov, S. M. Interaction of Zwitterionic Penicillins with the OmpF Channel Facilitates Their Translocation. *Biophys. J.* **2006**, *90*, 1617–1627.
- (18) Mach, T.; Neves, P.; Spiga, E.; Weingart, H.; Winterhalter, M.; Ruggerone, P.; Ceccarelli, M.; Gameiro, P. Facilitated Permeation of Antibiotics across Membrane Channels - Interaction of the Quinolone Moxifloxacin with the OmpF Channel. *J. Am. Chem. Soc.* **2008**, *130*, 13301–13309.
- (19) Ceccarelli, M.; Ruggerone, P. Physical Insights into Permeation of and Resistance to Antibiotics in Bacteria. *CDT* **2008**, *9*, 779–788.
- (20) Kumar, A.; Hajjar, E.; Ruggerone, P.; Ceccarelli, M. Molecular Simulations Reveal the Mechanism and the Determinants for Ampicillin Translocation through OmpF. *J. Phys. Chem. B* **2010**, *114*, 9608–9616.
- (21) Hajjar, E.; Bessonov, A.; Molitor, A.; Kumar, A.; Mahendran, K. R.; Winterhalter, M.; Pagès, J.-M.; Ruggerone, P.; Ceccarelli, M. Toward Screening for Antibiotics with Enhanced Permeation Properties through Bacterial Porins. *Biochemistry* **2010**, *49*, 6928–6935.
- (22) Van Den Berg, B.; Prathyusha Bhamidimarri, S.; Dahyabhai Prajapati, J.; Kleinekathöfer, U.; Winterhalter, M. Outer-Membrane Translocation of Bulky Small Molecules by Passive Diffusion. *Proc. Natl. Acad. Sci. U.S.A.* **2015**, *112*, E2991–E2999, DOI: [10.1073/pnas.1424835112](https://doi.org/10.1073/pnas.1424835112).
- (23) Samanta, S.; Bodrenko, I.; Acosta-Gutiérrez, S.; D'Agostino, T.; Pathania, M.; Ghai, I.; Schleberger, C.; Bumann, D.; Wagner, R.; Winterhalter, M.; Van Den Berg, B.; Ceccarelli, M. Getting Drugs through Small Pores: Exploiting the Porins Pathway in *Pseudomonas Aeruginosa*. *ACS Infect. Dis.* **2018**, *4*, 1519–1528.
- (24) Torrie, G. M.; Valleau, J. P. Monte Carlo free energy estimates using non-Boltzmann sampling: Application to the sub-critical Lennard-Jones fluid. *Chem. Phys. Lett.* **1974**, *28*, 578–581.
- (25) Laio, A.; Parrinello, M. Escaping Free-Energy Minima. *Proc. Natl. Acad. Sci. U.S.A.* **2002**, *99*, 12562–12566.
- (26) Golla, V. K.; Prajapati, J. D.; Joshi, M.; Kleinekathöfer, U. Exploration of Free Energy Surfaces across a Membrane Channel Using Metadynamics and Umbrella Sampling. *J. Chem. Theory Comput.* **2020**, *16*, 2751–2765.
- (27) Kumar Golla, V.; Piselli, C.; Kleinekathöfer, U.; Benz, R. Permeation of Fosfomycin through the Phosphate-Specific Channels OprP and OprO of *Pseudomonas aeruginosa*. *J. Phys. Chem. B* **2022**, *126*, 1388–1403.
- (28) Pira, A.; Scorciapino, M. A.; Bodrenko, I. V.; Bosin, A.; Acosta-Gutiérrez, S.; Ceccarelli, M. Permeation of β -lactamase inhibitors through the general porins of gram-negative bacteria. *Molecules* **2020**, *25*, No. 5747, DOI: [10.3390/molecules25235747](https://doi.org/10.3390/molecules25235747).
- (29) Sugita, Y.; Kitao, A.; Okamoto, Y. Multidimensional replica-exchange method for free-energy calculations. *J. Chem. Phys.* **2000**, *113*, 6042–6051.
- (30) Wang, L.; Friesner, R. A.; Berne, B. J. Replica Exchange with Solute Scaling: A More Efficient Version of Replica Exchange with Solute Tempering (REST2). *J. Phys. Chem. B* **2011**, *115*, 9431–9438.
- (31) Bussi, G. Hamiltonian replica exchange in GROMACS: A flexible implementation. *Mol. Phys.* **2014**, *112*, 379–384.
- (32) Awasthi, S.; Nair, N. N. Exploring high dimensional free energy landscapes: Temperature accelerated sliced sampling. *J. Chem. Phys.* **2017**, *146*, No. 094108.
- (33) Sousa, C. F.; Becker, R. A.; Lehr, C.-M.; Kalinina, O. V.; Hub, J. S. Simulated tempering-enhanced umbrella sampling improves convergence of free energy calculations of drug membrane permeation. *J. Chem. Theory Comput.* **2023**, 1898–1907, DOI: [10.1021/acs.jctc.2c01162](https://doi.org/10.1021/acs.jctc.2c01162).
- (34) Haloi, N.; Vasan, A. K.; Geddes, E. J.; Prasanna, A.; Wen, P. C.; Metcalf, W. W.; Hergenrother, P. J.; Tajkhorshid, E. Rationalizing the generation of broad spectrum antibiotics with the addition of a positive charge. *Chem. Sci.* **2021**, *12*, 15028–15044.
- (35) Vasan, A. K.; Haloi, N.; Ulrich, R. J.; Metcalf, M. E.; Wen, P. C.; Metcalf, W. W.; Hergenrother, P. J.; Shukla, D.; Tajkhorshid, E. Role of internal loop dynamics in antibiotic permeability of outer membrane porins. *Proc. Natl. Acad. Sci. U.S.A.* **2022**, *119*, No. e2117009119.
- (36) Acharya, A.; Prajapati, J. D.; Kleinekathöfer, U. Improved sampling and free energy estimates for antibiotic permeation through bacterial porins. *J. Chem. Theory Comput.* **2021**, *17*, 4564–4577.
- (37) Marinari, E.; Parisi, G. Simulated tempering: A New Monte Carlo Scheme. *Europhys. Lett.* **1992**, *19*, 451–458.
- (38) Abraham, M. J.; Murtola, T.; Schulz, R.; Páll, S.; Smith, J. C.; Hess, B.; Lindah, E. GROMACS: High performance molecular simulations through multi-level parallelism from laptops to supercomputers. *SoftwareX* **2015**, *1–2*, 19–25.
- (39) Tribello, G. A.; Bonomi, M.; Branduardi, D.; Camilloni, C.; Bussi, G. PLUMED 2: New feathers for an old bird. *Comput. Phys. Commun.* **2014**, *185*, 604–613.
- (40) Bonomi, M.; Bussi, G.; Camilloni, C.; Tribello, G. A.; Banáš, P.; Barducci, A.; Bernetti, M.; Bolhuis, P. G.; Bottaro, S.; Branduardi, D.; Capelli, R.; Carloni, P.; Ceriotti, M.; Cesari, A.; Chen, H.; Chen, W.;

- Colizzi, F.; De, S.; De La Pierre, M.; Donadio, D.; Drobot, V.; Ensing, B.; Ferguson, A. L.; Filizola, M.; Fraser, J. S.; Fu, H.; Gasparotto, P.; Gervasio, F. L.; Giberti, F.; Gil-Ley, A.; Giorgino, T.; Heller, G. T.; Hocky, G. M.; Iannuzzi, M.; Invernizzi, M.; Jelfs, K. E.; Jussupow, A.; Kirilin, E.; Laio, A.; Limongelli, V.; Lindorff-Larsen, K.; Löhr, T.; Marinelli, F.; Martin-Samos, L.; Masetti, M.; Meyer, R.; Michaelides, A.; Molteni, C.; Morishita, T.; Nava, M.; Paissoni, C.; Papaleo, E.; Parrinello, M.; Pfaendtner, J.; Piaggi, P.; Piccini, G. M.; Pietropaolo, A.; Pietrucci, F.; Pipolo, S.; Provasi, D.; Quigley, D.; Raiteri, P.; Raniolo, S.; Rydzewski, J.; Salvalaglio, M.; Sosso, G. C.; Spiwok, V.; Šponer, J.; Swenson, D. W.; Tiwary, P.; Valsson, O.; Vendruscolo, M.; Voth, G. A.; White, A. Promoting transparency and reproducibility in enhanced molecular simulations. *Nat. Methods* **2019**, *16*, 670–673.
- (41) Modi, N.; Ganguly, S.; Bárcena-Urbarri, I.; Benz, R.; Van Den Berg, B.; Kleinekathöfer, U. Structure, dynamics, and substrate specificity of the OprO porin from *Pseudomonas aeruginosa*. *Biophys. J.* **2015**, *109*, 1429–1438.
- (42) Klauda, J. B.; Venable, R. M.; Freites, J. A.; O'Connor, J. W.; Tobias, D. J.; Mondragon-Ramirez, C.; Vorobyov, I.; MacKerell, A. D.; Pastor, R. W. Update of the CHARMM All-Atom Additive Force Field for Lipids: Validation on Six Lipid Types. *J. Phys. Chem. B* **2010**, *114*, 7830–7843.
- (43) Vanommeslaeghe, K.; Hatcher, E.; Acharya, C.; Kundu, S.; Zhong, S.; Shim, J.; Darian, E.; Guvench, O.; Lopes, P.; Vorobyov, I.; Mackerell, A. D. CHARMM general force field: A force field for drug-like molecules compatible with the CHARMM all-atom additive biological force fields. *J. Comput. Chem.* **2010**, *31*, 671–690.
- (44) Jo, S.; Kim, T.; Iyer, V. G.; Im, W. CHARMM-GUI: A web-based graphical user interface for CHARMM. *J. Comput. Chem.* **2008**, *29*, 1859–1865.
- (45) Jorgensen, W. L.; Chandrasekhar, J.; Madura, J. D.; Impey, R. W.; Klein, M. L. Comparison of simple potential functions for simulating liquid water. *J. Chem. Phys.* **1983**, *79*, 926–935, DOI: 10.1063/1.445869.
- (46) Darden, T.; York, D.; Pedersen, L. Particle mesh Ewald: An $N \log(N)$ method for Ewald sums in large systems. *J. Chem. Phys.* **1993**, *98*, 10089–10092.
- (47) Miyamoto, S.; Kollman, P. A. Settle: An analytical version of the SHAKE and RATTLE algorithm for rigid water models. *J. Comput. Chem.* **1992**, *13*, 952–962.
- (48) Hess, B.; Bekker, H.; Berendsen, H. J. C.; Fraaije, J. G. E. M. LINCS: A Linear Constraint Solver for Molecular Simulations. *J. Comput. Chem.* **1997**, *18*, 1463–1472.
- (49) Berendsen, H. J. C.; Postma, J. P.; Van Gunsteren, W. F.; Dinola, A.; Haak, J. R. Molecular dynamics with coupling to an external bath. *J. Chem. Phys.* **1984**, *81*, 3684–3690.
- (50) Parrinello, M.; Rahman, A. Polymorphic transitions in single crystals: A new molecular dynamics method. *J. Appl. Phys.* **1981**, *52*, 7182.
- (51) Bussi, G.; Donadio, D.; Parrinello, M. Canonical sampling through velocity rescaling. *J. Chem. Phys.* **2007**, *126*, No. 014101.
- (52) Park, S.; Pande, V. S. Choosing weights for simulated tempering. *Phys. Rev. E* **2007**, *76*, No. 016703, DOI: 10.1103/PhysRevE.76.016703.
- (53) Grubmüller, H.; Heymann, B.; Tavan, P. Ligand Binding: Molecular Mechanics Calculation of the Streptavidin-Biotin Rupture Force. *Science* **1996**, *271*, 997–999.
- (54) Leech, J.; Prins, J. F.; Hermans, J. SMD: Visual steering of molecular dynamics for protein design. *IEEE Comput. Sci. Eng.* **1996**, *3*, 38–45.
- (55) Ferreira, R. J.; Kasson, P. M. Antibiotic Uptake Across Gram-Negative Outer Membranes: Better Predictions Towards Better Antibiotics. *ACS Infect. Dis.* **2019**, *5*, 2096–2104.
- (56) Virtanen, P.; Gommers, R.; Oliphant, T. E.; Haberland, M.; Reddy, T.; Cournapeau, D.; Burovski, E.; Peterson, P.; Weckesser, W.; Bright, J.; van der Walt, S. J.; Brett, M.; Wilson, J.; Millman, K. J.; Mayorov, N.; Nelson, A. R.; Jones, E.; Kern, R.; Larson, E.; Carey, C. J.; Polat, F.; Feng, Y.; Moore, E. W.; VanderPlas, J.; Laxalde, D.; Perktold, J.; Cimrman, R.; Henriksen, I.; Quintero, E. A.; Harris, C. R.; Archibald, A. M.; Ribeiro, A. H.; Pedregosa, F.; van Mulbregt, P.; Vijaykumar, A.; Bardelli, A. P.; Rothberg, A.; Hilboll, A.; Kloeckner, A.; Scopatz, A.; Lee, A.; Rokem, A.; Woods, C. N.; Fulton, C.; Masson, C.; Häggström, C.; Fitzgerald, C.; Nicholson, D. A.; Hagen, D. R.; Pasechnik, D. V.; Olivetti, E.; Martin, E.; Wieser, E.; Silva, F.; Lenders, F.; Wilhelm, F.; Young, G.; Price, G. A.; Ingold, G. L.; Allen, G. E.; Lee, G. R.; Audren, H.; Probst, I.; Dietrich, J. P.; Silterra, J.; Webber, J. T.; Slavič, J.; Nothman, J.; Buchner, J.; Kulick, J.; Schönberger, J. L.; de Miranda Cardoso, J. V.; Reimer, J.; Harrington, J.; Rodriguez, J. L. C.; Nunez-Iglesias, J.; Kuczynski, J.; Tritz, K.; Thoma, M.; Newville, M.; Kümmerer, M.; Bolingbroke, M.; Tartre, M.; Pak, M.; Smith, N. J.; Nowaczyk, N.; Shebanov, N.; Pavlyk, O.; Brodtkorb, P. A.; Lee, P.; McGibbon, R. T.; Feldbauer, R.; Lewis, S.; Tygier, S.; Sievert, S.; Vigna, S.; Peterson, S.; More, S.; Pudlik, T.; Oshima, T.; Pingel, T. J.; Robitaille, T. P.; Spura, T.; Jones, T. R.; Cera, T.; Leslie, T.; Zito, T.; Krauss, T.; Upadhyay, U.; Halchenko, Y. O.; Vázquez-Baeza, Y. SciPy 1.0: fundamental algorithms for scientific computing in Python. *Nat. Methods* **2020**, *17*, 261–272.
- (57) Metropolis, N.; Rosenbluth, A. W.; Rosenbluth, M. N.; Teller, A. H.; Teller, E. Equation of state calculations by fast computing machines. *J. Chem. Phys.* **1953**, *21*, 1087–1092.
- (58) Jiang, W.; Luo, Y.; Maragliano, L.; Roux, B. Calculation of Free Energy Landscape in Multi-Dimensions with Hamiltonian-Exchange Umbrella Sampling on Petascale Supercomputer. *J. Chem. Theory Comput.* **2012**, *8*, 4672–4680.
- (59) Awasthi, N.; Hub, J. S. Simulations of Pore Formation in Lipid Membranes: Reaction Coordinates, Convergence, Hysteresis, and Finite-Size Effects. *J. Chem. Theory Comput.* **2016**, *12*, 3261–3269.
- (60) Lichtinger, S. M.; Biggin, P. C. Tackling Hysteresis in Conformational Sampling – How to Be Forgetful with MEMENTO. *J. Chem. Theory Comput.* **2023**, 3705–3720, DOI: 10.1021/acs.jctc.3c00140.
- (61) Pan, A. C.; Weinreich, T. M.; Piana, S.; Shaw, D. E. Demonstrating an Order-of-Magnitude Sampling Enhancement in Molecular Dynamics Simulations of Complex Protein Systems. *J. Chem. Theory Comput.* **2016**, *12*, 1360–1367.
- (62) Shrestha, U. R.; Juneja, P.; Zhang, Q.; Gurumoorthy, V.; Borroguero, J. M.; Urban, V.; Cheng, X.; Pingali, S. V.; Smith, J. C.; O'Neill, H. M.; Petridis, L. Generation of the Configurational Ensemble of an Intrinsically Disordered Protein from Unbiased Molecular Dynamics Simulation. *Proc. Natl. Acad. Sci. U.S.A.* **2019**, *116*, 20446–20452.
- (63) Becker, R. A.; Hub, J. S. Continuous Millisecond Conformational Cycle of a DEAH Box Helicase Reveals Control of Domain Motions by Atomic-Scale Transitions. *Commun. Biol.* **2023**, *6*, No. 379.
- (64) Bodrenko, I. V.; Salis, S.; Acosta-Gutierrez, S.; Ceccarelli, M. Diffusion of large particles through small pores: From entropic to enthalpic transport. *J. Chem. Phys.* **2019**, *150*, No. 211102, DOI: 10.1063/1.5098868.
- (65) Milenkovic, S.; Wang, J.; Acosta-Gutierrez, S.; Winterhalter, M.; Ceccarelli, M.; Bodrenko, I. V. How the Physical Properties of Bacterial Porins Match Environmental Conditions. *Phys. Chem. Chem. Phys.* **2023**, *25*, 12712–12722.
- (66) Awoonor-Williams, E.; Rowley, C. N. Molecular Simulation of Nonfacilitated Membrane Permeation. *Biochim. Biophys. Acta, Biomembr.* **2016**, *1858*, 1672–1687.
- (67) Song, L. F.; Merz, K. M. Evolution of Alchemical Free Energy Methods in Drug Discovery. *J. Chem. Inf. Model.* **2020**, *60*, 5308–5318.
- (68) Ahmed, M. C.; Papaleo, E.; Lindorff-Larsen, K. How Well Do Force Fields Capture the Strength of Salt Bridges in Proteins? *PeerJ* **2018**, *6*, No. e4967.